

The Effect of Cu on the Decomposition of Al-Zn-Mg-(Cu) Alloys

Lamb J^{1*} and Sanders Jr. TH²

¹Universal Alloy Corporation, Canton, Georgia 30114, USA

²School of Materials Science and Engineering, Georgia Institute of Technology, Atlanta, Georgia, USA

Abstract

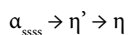
A series of experimental Al-Zn-Mg-(Cu) alloys with a semi-constant Zn:Mg ratio were produced via hot rolling. The effects of Cu in these alloys on the activation energy for precipitation, the response to natural aging, the size of the precipitate free zone, and the corrosion resistance were investigated.

Keywords: Precipitation; Homogenous; Morphology; Quenching

Introduction

The precipitation hardenable 7xxx-series of aluminum alloys, which is based on either the ternary Al-Zn-Mg or the quaternary Al-Zn-Mg-Cu system, are extensively utilized for structural components in aerospace applications due to their high specific strength [1,2]. The precipitation process in Al-Zn-Mg-Cu alloys is highly complex consisting of both homogenous and heterogeneous nucleation and growth reactions. For example the precipitation of Guinier-Preston (GP) zones at room temperature is essentially a homogenous process, while the transformation of GP-zones into η' and η is a heterogeneous process. Additionally the direct nucleation of η' and η is also a heterogeneous process [3].

The precipitation processes most referenced for 7xxx-series alloys are:



However, recent literature suggests this is an incomplete description because the roles of vacancy rich clusters (VRC) and dislocations are ignored. Furthermore, two distinct types of GP zones (GP-I and GP-II) are known to occur, but the delineation of the two is negated above [4,5]. Processing parameters such as solution heat treatment (SHT) and stretching are also known to alter the precipitation process in 7xxx-series alloys [6-8].

Modern high-strength 7xxx-series aluminum alloys like AA7136 are typically alloyed with Cu to increase strength and SCC resistance [6]. Copper additions to 7xxx-series alloys are known to change the morphology of GP-zones and raise the GP-zone solvus temperature [9]. For example, Chinh et al. [10] observed that in Al-Zn-Mg alloys GP-zones were mostly spherical in nature, but in Al-Zn-Mg-Cu alloys two distinct types of GP-zones formed: spherical and ellipsoidal. It has also been shown that Cu additions can increase the aging kinetics and quench sensitivity of an Al-Zn-Mg alloy [6].

Clinch et al. [5] provided a systematic detailed study on the effects of the Zn:Mg ratio and total solute content on the aging process in 7xxx-series alloys; however, Clinch et al. neglected to stretch their alloys, a process which is known to increase coarsening kinetics, and held Cu content constant. Newer 7xxx-series alloys like AA7136 have higher Zn and Mg contents than those studied by Clinch as well. Therefore, it is important for the effect of Cu content on these high solute alloys be systematically studied.

In order to systematically quantify the effects of Cu additions

on these newer high-strength aluminum alloys, which typically have higher Zn and Mg contents than more traditional alloys like AA7075 and AA7050, a series of experimental alloys with a semi-constant Zn:Mg ratio were cast with various amounts of Cu. The effects of Cu on the activation energy for precipitation in each alloy was then determined via DSC and the effects of natural aging on the T6 and T7 tempers was established. TEM was utilized to determine the precipitate free zone (PFZ) size along the grain boundaries in each alloy in an attempt to correlate Cu content to PFZ size. Furthermore, the effects of Cu additions on the EXCO and IGC resistance of the alloys in the T7 temper were studied.

Materials and Methods

A series of five experimental alloys were cast (Table 1) and homogenized at 440°C for 24 hours. The alloys were subsequently rolled at 343°C to a 60% reduction before being solution heat treated at 470°C, water quenched, and stretch 1.5%. The alloys were then allowed to naturally age for 0-96 hours before being artificially aged. To produce the T6 temper the alloys were aged for 24 hours at 120°C, and a T7 temper was produced by further aging the alloys at 160°C for 24 hours. It should be noted that this results in an extremely over-aged condition resembling an industrial T73x product.

Micrographs of alloys I-V were taken at 50x in the L-S direction using a Leica CTR6500. The micrographs were etched using Barker's Reagent. The effects of natural aging prior to artificial aging were studied using Rockwell hardness (B-scale) measurements in conjunction with DSC analysis.

DSC scans from 50°C to 515°C using scan rates of 5, 10, 20, and 50°C/min were conducted on each alloy in the W-temper using a Perkin-Elmer DSC 8000. The Augis and Bennet expression was then utilized to determine the activation energies for precipitation in each alloy (Table 2) [11]:

$$\ln\left(\frac{r}{T_p - T_0}\right) = \ln A - \frac{Q}{RT_p}$$

***Corresponding author:** Justin Lamb, Research Scientist and CAE, Universal Alloy Corporation, 180 Lamar-Haley Pkwy, Canton, GA 30114, USA, Tel: (770) 479-7230; E-mail: Justin.Lamb@universalalloy.com

Received November 22, 2017; **Accepted** December 11, 2017; **Published** December 21, 2017

Citation: Lamb J, Sanders JTH (2017) The Effect of Cu on the Decomposition of Al-Zn-Mg-(Cu) Alloys. J Material Sci Eng 6: 404. doi: [10.4172/2169-0022.1000404](https://doi.org/10.4172/2169-0022.1000404)

Copyright: © 2017 Lamb J, et al. This is an open-access article distributed under the terms of the Creative Commons Attribution License, which permits unrestricted use, distribution, and reproduction in any medium, provided the original author and source are credited.

Alloy	Si	Fe	Zn	Mg	Cu	Zn:Mg
I	0.04	0.03	4.02	2.39	1.38	1.68
II	0.04	0.03	4.11	2.48	0.83	1.66
III	0.04	0.03	4.05	2.46	0.56	1.64
IV	0.03	0.03	3.84	2.45	0.25	1.57
V	0.03	0.03	3.89	2.45	0.00	1.59

Table 1: Chemical composition of the investigated aluminum alloys at.%.

Alloy	(Zn+Cu):Mg (at.%)	Q(η') (kJ/mol)	Q(η) (kJ/mol)	Q(T) (kJ/mol)
I	2.26	70.25	80.56	76.59
II	1.99	81.91	88.32	75.42
III	1.87	106.59	104.32	96.50
IV	1.67	-	84.06	90.82
V	1.59	-	81.24	78.23

Table 2: Activation energies for precipitation in Alloys I-V by precipitate.

Where T_p is the peak temperature of the DSC curves, T_0 is the initial temperature, r is the heating rate, A is the reaction rate, Q is the activation energy, and R is the universal gas constant. Plotting $\ln[r/(T_p - T_0)]$ versus $1/(T_p R)$ should yield a straight line of slope equal to Q (i.e. - the activation energy for precipitation in the W-temper).

The average PFZ size of each alloy in the T7 condition was determined via TEM. TEM foils were prepared by jet polishing 3 mm disc using a 75% methanol-25% nitric solution at -20°C and images were taken on a 100 KV Hitachi HT7700.

Exfoliation corrosion (EXCO) testing was conducted according to ASTM G34 at a depth of T/10 [12]. It should be noted, however, that samples did not meet the minimum test area required by ASTM G34. Likewise, Intergranular corrosion (IGC) testing was conducted according to ASTM G1110 at a depth of T/10 [13]. The frequency of IGC attacks was calculated by dividing the number of attacks across the surface of the samples by the measured distance across each sample in the T-S direction.

Results

Starting microstructure

Micrographs (Barker's Reagent) of Alloys I-V were taken in the L-S direction at 100x. The microstructures of Alloys I-V, an example of which can be seen in Figure 1, appear to be completely recrystallized (REX). This is evident by the lack of sub-grain structure present in the microstructures. The REX microstructure is probably due to the fact that Alloys I-V do not contain any dispersoid forming elements (ex. - Zr, Cr, Sc, etc.).

The effects of Cu on the activation energy for precipitation

The activation energy for the precipitation of η' , η , and T-phase in Alloys I-V was determined using DSC via the Augis and Bennet expression. The peak precipitation temperature for each precipitate (T_p) was determined using the Pyris software and used to plot $\ln[r/(T_p - T_0)]$ versus $1/(T_p R)$ as can be seen for Alloy I in Figure 2. The activation energy was then determined via a linear fit of the data. The activation energy for precipitation in Alloys I-V by precipitate can be seen in Table 3. These values can be seen plotted against each alloys (Zn+Cu):Mg ratio (at.%) in Figure 3.

It is clear from Figure 3 that Cu content has a direct effect on the activation energy for precipitation in 7xxx-series alloys. For example, as Cu content is increased the activation energy for η' precipitation becomes much lower than for that of η , which is due to the increased

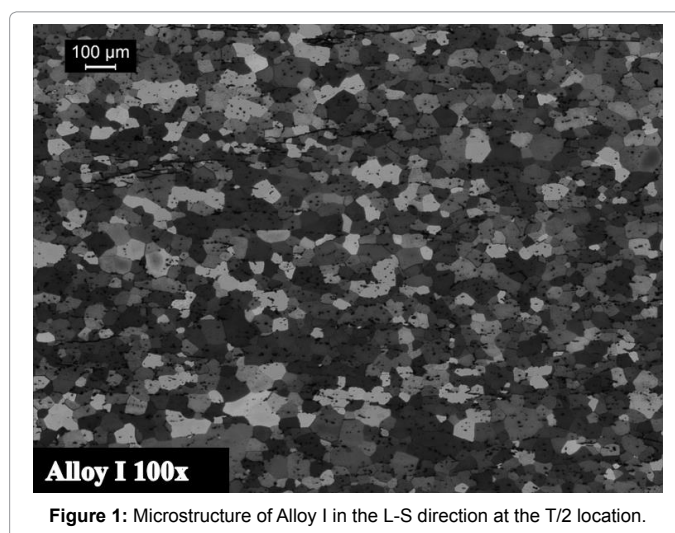


Figure 1: Microstructure of Alloy I in the L-S direction at the T/2 location.

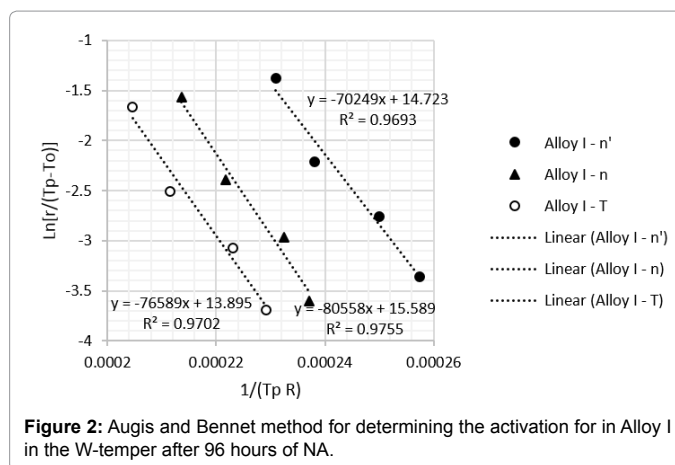


Figure 2: Augis and Bennet method for determining the activation for in Alloy I in the W-temper after 96 hours of NA.

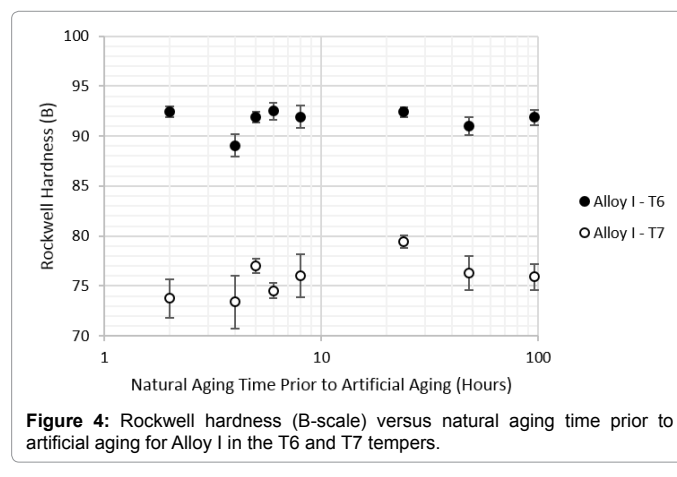
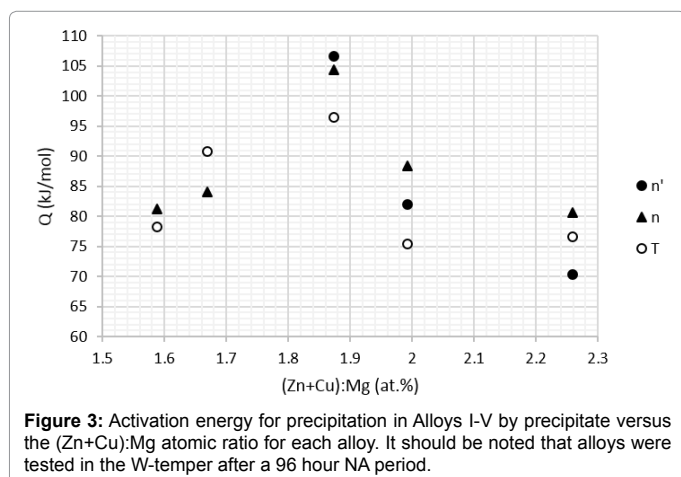
lattice strain from the Cu atoms. Interestingly, there appears to be a critical Cu content for a given Zn:Mg ratio where the activation energy for η' and η are essentially equal (i.e. Alloy III), but it should be noted that the DSC scans still clearly show an η' peak.

For low Cu alloys like Alloys IV and V, which are below this point, the η' precipitation peak is not distinguishable in the DSC scans. This would seem to suggest that either the activation energy for η' is larger than that for η making it unfavorable thermodynamically, or due to

Alloy	NA Time (Hrs)	T6			T7		
		η'	η	T	η'	η	T
I	2	216	253	279	-	266	-
	8	217	253	-	-	265	-
	96	216	255	-	242	278	302
II	2	221	247	274	-	269	361
	8	224	248	265	237	273	-
	96	222	247	265	236	274	340
III	2	225	247	273	-	277	344
	8	226	246	267	-	278	-
	96	227	247	273	236	274	-
IV	2	226	249	-	-	269	335
	8	227	246	266	238	273	-
	96	229	246	-	-	274	-
V	2	228	247	274	248	280	-
	8	-	246	267	-	272	-
	96	-	246	274	241	271	-

Note: “-”denotes a peak was not observed.

Table 3: Peak precipitation temperatures (°C) from DSC scans on Alloys I-V in both the T6 and T7 condition from 50-515°C at 20°C/min.



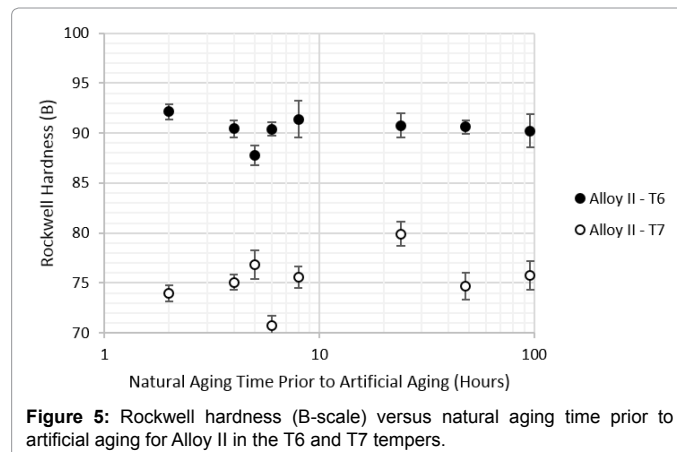
the fact that GP-zones in low-Cu alloys are not stabilized that the η' reaction happens so quickly it was not distinguishable in the DSC scans. The fact that the activation energy for η precipitation begins to decrease after the Cu content drops below the critical Cu-content could also be related to the type of GP-zones present in the microstructure. For example, it is known that η can precipitate directly onto GP-I zones unlike η' . Furthermore, GP-II zones are generally thought to require more lattice strain (i.e. increased Cu contents) to form.

T-phase ($AlMg_3Zn_3$) also appears to follow a similar pattern to η with respect to changes in its activation energy. It is known that T-phase has some solubility for Cu much like η' and η so these results are not unexpected. The fact that in Alloy IV the activation energy for T-phase is higher than η could be related to the Zn:Mg ratio, which is known to directly affect the main precipitate-type (i.e. – T-phase or η) in 7xxx-series alloys [14].

The effects of Cu on the response to natural aging

The effects of Cu on the response to natural aging prior to artificial aging in the T6 and T7 tempers were studied via DSC and Rockwell hardness. Figures 4-8 display Rockwell hardness measurements versus NA time for Alloys I-V, respectively, in the T6 and T7 tempers.

With respect to the T6 temper, the high Cu alloys, Alloys I (1.38



at.%) and II (0.83 at.%), appear to show a decrease in strength with increased natural aging time. This is not unexpected as the GP-I zones, which form during the natural aging period, are stabilized by the strain induced by the Cu additions to the point where they are stable past the GP-II zone precipitation temperature (and potentially the η' precipitation temperature), effectively lowering the strength in the T6 temper. Both alloys also appear to show a dip in hardness at low natural

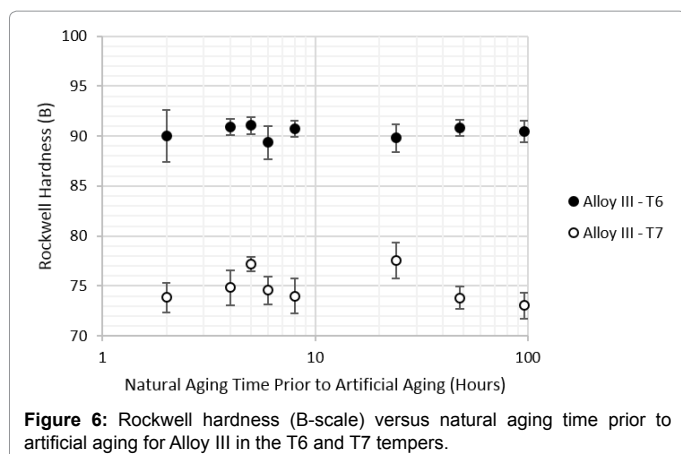


Figure 6: Rockwell hardness (B-scale) versus natural aging time prior to artificial aging for Alloy III in the T6 and T7 tempers.

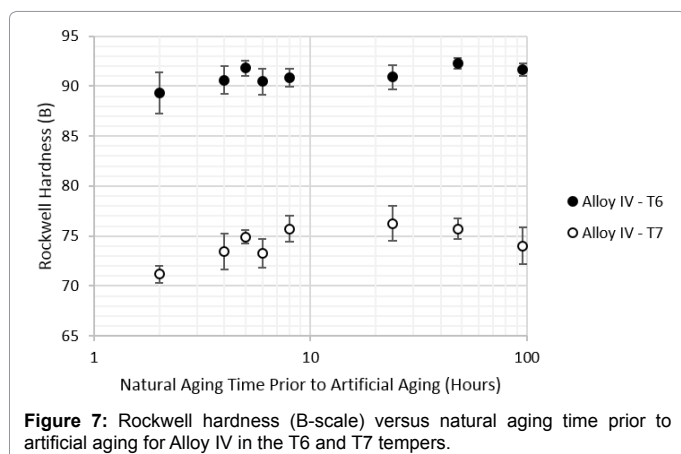


Figure 7: Rockwell hardness (B-scale) versus natural aging time prior to artificial aging for Alloy IV in the T6 and T7 tempers.

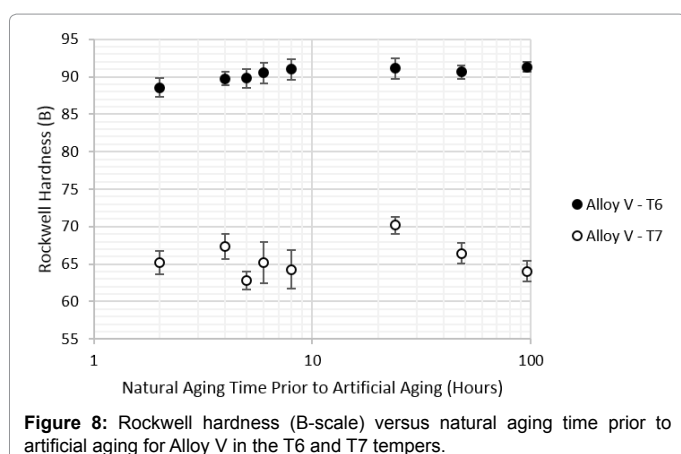


Figure 8: Rockwell hardness (B-scale) versus natural aging time prior to artificial aging for Alloy V in the T6 and T7 tempers.

aging time, which is a known characteristic of AA7075, and could be the result of a transitional period in GP-zone formation [6].

Alloy III (0.56 at.%) appears to have a neutral response to natural aging in the T6 temper. This suggests that the rates of GP-I zone stabilization and reversion are balanced. Conversely, Alloys IV (0.25 at.%) and V (0.00 at.%) display an increase in hardness with increased natural aging time. There is research to suggest that subjecting a low-Cu 7xxx-series alloys to a natural aging period prior to artificial aging promotes the growth of a fine, homogenous dispersion of GP-I zones [7,15]. In theory, the GP-I zones precipitated out during natural aging

would quickly dissolve back into solution and create a fine dispersion of concentrate solute upon which GP-II zones/ η' can precipitate.

Interestingly, the data appears to indicate that Cu may not directly affect the hardness of 7xxx-series alloys in extremely over-aged products (i.e. – T73x). The response to natural aging in the T7 temper for Alloys I-V appears to be similar. The hardness gradually increases with natural aging time to a peak before decreasing. This is probably due to nucleation and growth mechanisms associated with GP-I zone precipitation. The number of GP-I zones appears to increase until a maximum is reached at which the larger GP-I zones begin to coarsen at the expense of smaller GP zones. The fact that most documented precipitation process, even those not containing GP-II zones or η' , end with η is probably the reason the effects of Cu are masked in the T7 temper. Although, it should be noted that shorter over-aging practices (ex. – T79x, T76x, T74x) may show more sensitivity to Cu content.

The DSC data for Alloys I-V in the T6 and T7 tempers can be seen in Table 3. Alloys I and II NA 8 hours prior to aging to the T6 temper appear to show a slight increase in the η' precipitation temperature compared to the 2 and 9 hours samples. This appears to correlate to the lower hardness observed in the 8 hours samples (i.e. – the “AA7075 behavior”). The η' precipitation peak in Alloys III and IV, conversely, appear to increase in a linear fashion with increased NA time. With respect to Alloy V, an η' precipitation peak was only observed in the 2 hours sample in the T6 temper. Interestingly, in the T7 temper most of the η' precipitation peaks appear to disappear regardless of alloy, although most of the 96 hour NA samples did display an η' precipitation peak.

With respect to the η precipitation peak, Alloy I appears to show no change with respect to NA in the T6 temper, although the precipitation peak appears to shift to a higher temperature at longer NA times in the T7 temper. Alloys II and III appear to show an inverse relationship with respect to η precipitation peaks (ex. – in Alloy II-T7 the highest η peak observed was at 96 hours of NA whereas for Alloy III-T7 it was at 2 hours NA). This is significant as it may denote a shift in the effects of Cu and NA on the precipitation process, and Alloys IV and V appear to follow suite with Alloy III.

The effects of Cu on the size of the precipitate free zone

The effects of Cu on the size of the precipitate free zone (PFZ) in T7 condition was evaluated via TEM. Table 4 shows the average measured PFZ in each alloy. Figures 9 and 10 show typical grain boundaries and PFZs in Alloys I and V, respectively. The effect of Cu on the morphology of grain boundary η is apparent with the Cu-free Alloy V displaying spherical or ellipsoidal η precipitates, and 1.38 at.% Cu Alloy I displaying lenticular η precipitates in the grain boundary.

Unfortunately, a direct correlation between Cu content and average PFZ width could not be made. This could be due to several factors including the lack of dispersoid elements, which are known to trap vacancies in the matrix from migrating to the grain boundaries, but appears to suggest that the Cu content in properly quenched samples plays little role in determining the PFZ width, especially in the T7

Alloy	Cu Content (at.%)	<PFZ>
I	1.38	22.9 ± 10.1 nm
II	0.83	26.0 ± 9.6 nm
III	0.56	20.0 ± 10.3 nm
IV	0.25	45.7 ± 20.5 nm
V	0.00	22.4 ± 9.0 nm

Table 4: Average PFZ width along grain boundaries in Alloys I-V.

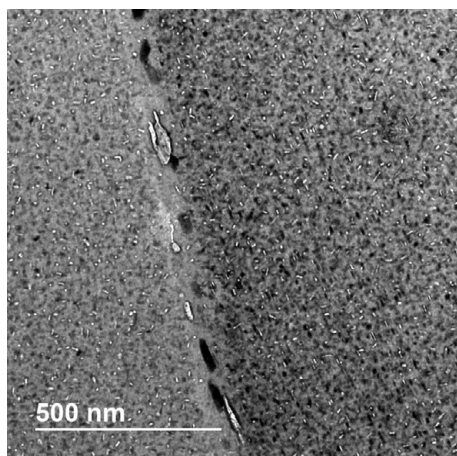


Figure 9: TEM image of GT1-T7.

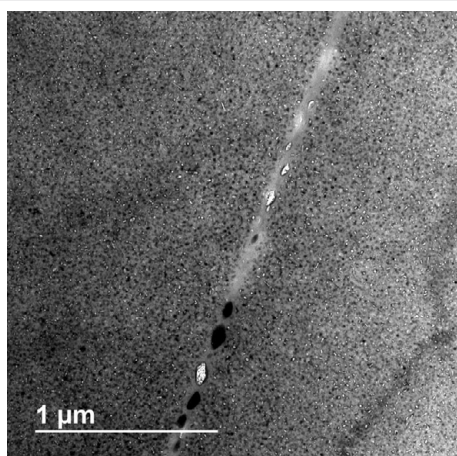


Figure 10: TEM image of GT5-T7.

temper. Therefore, the increase in SCC resistance attributed to Cu additions maybe more electrochemical in nature as Cu, along with Al, is known to alter the composition of η by substituting for Zn to form $Mg(Zn, Al, Cu)_2$.

The effects of Cu on exfoliation corrosion (EXCO) and intergranular corrosion (IGC) resistance

The EXCO and IGC resistance of Alloys I-V were determined via ASTM G34 and G110, respectively. The results of the EXCO testing can be seen in Table 5. Figure 11 displays the maximum IGC attack observed and the frequency of IGC attack versus the Cu contents of Alloys I-V.

As expected, the resistance to EXCO appears to decrease with increasing Cu content. This is evident with respect to both the ASTM G34 rating and the weight loss over the 48 hour exposure. Compositional ranges of equal susceptibility can also be determined from the data presented in Table 5. Typically, an EXCO rating of EA in any temper is considered good for a high strength 7xxx-series product. Table 5 suggests that almost 2 wt.% Cu can be added to a high strength alloy before an ASTM G34 rating of EB is observed. This means that substantial gains in strength can be made with Cu additions without sacrificing EXCO resistance.

The IGC resistance also appears to be directly correlated to the

Alloy	Test Area (cm ²)	Weight Loss (g/cm ²)	ASTM G34 Rating
I	1.57	0.06	EB
II	1.95	0.03	EA
III	1.16	0.01	EA
IV	2.04	0.01	P
V	0.77	0.01	N

Table 5: Results of EXCO testing (ASTM G34) on Alloys I-V in the T7 temper.

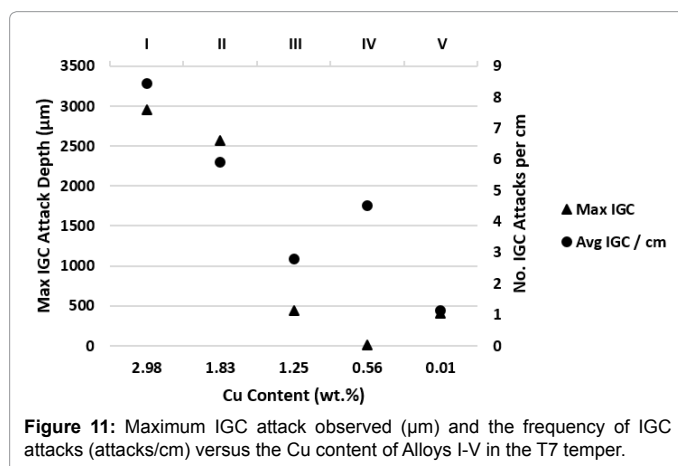


Figure 11: Maximum IGC attack observed (μm) and the frequency of IGC attacks (attacks/cm) versus the Cu content of Alloys I-V in the T7 temper.

Cu content. There appears to be a semi-linear relationship between the Cu content and the maximum IGC attack observed as well as the frequency of attack.

Conclusions

The effects of Cu content on the decomposition of Al-Zn-Mg-Cu were studied via DSC, hardness, TEM, and corrosion testing. It was shown that Cu additions to 7xxx-series alloys with a high Zn and Mg contents such that the Zn:Mg (at.%) is approximately equal to 1.6 had the following effects:

- The Cu content of a 7xxx-series alloy appears to affect the response to NA prior to artificial aging in T6 products. Low Cu products have a positive response to NA in the T6 temper, whereas high Cu products appear to have a negative response in the T6 temper.
- Conversely, the effects of NA appear to disappear in extremely over-aged products (i.e. – T73 tempers), although the effects may still be seen in less over-aged products.
- The width of the PFZ around grain boundary precipitates appears to not be directly related to Cu content, although the morphology of the grain boundary precipitates was shown to be altered. This could be due to several factors including temper and proper quenching from SHT.
- EXCO and IGC resistance were shown to decrease with increasing Cu content.

References

1. Sanders Jr. T, Sawtell R, Staley J, Buccie R, Thakker A (1978) Effect of microstructure on fatigue crack growth of 7xxx aluminum alloys under constant amplitude and spectrum loading. ASA057129, Alcoa, Pittsburgh, PA.
2. Hunsicker H (1976) Development of Al-Zn-Mg-Cu alloys for aircraft. Philosophical Transactions of the Royal Society of London Series A, Mathematical and Physical Sciences 282: 359-376.
3. Sanders Jr. T, Starke Jr. E (1976) The relationship of microstructure to

- monotonic and cyclic straining of two age hardening aluminum alloys. Metallurgical Transactions A 7: 1407-1418.
4. Berg L, Gjønnnes J, Hansen V, Li Z, Knutson-Wedel M, et al. (2001) GP-zones in Al-Zn-Mg alloys and their role in artificial aging. Acta Materialia 49: 3443-3451.
 5. Clinch M, Harris S, Hepples W, Holroyd N, Lawday M, et al. (2006) Influence of zinc to magnesium ratio and total solute content on the strength and toughness of 7xxx-series alloys. Materials Science Forum 519-521: 339-344.
 6. Hatch J (1984) Aluminum: Properties and Physical Metallurgy. ASM, Metals Park, Ohio.
 7. Deschamps A, Livet F, Brechet Y (1998) Influence of predeformation on ageing in an Al-Zn-Mg alloy I: microstructure evolution and mechanical properties. Acta Materialia 47: 281-292.
 8. Deschamps A, Brechet Y (1998) Influence of predeformation on ageing in an Al-Zn-Mg alloy II: modeling precipitation kinetics and yield stress. Acta Materialia 47: 293-305.
 9. Staley J (1974) Aging kinetics of aluminum alloy 7050. Metallurgical Transactions 5: 929-932.
 10. Chinh N, Lendvai J, Ping D, Hono K (2004) The effect of Cu on mechanical and precipitation properties of Al-Zn-Mg alloys. Journal of Alloys and Compounds 378: 52-60.
 11. Augis J, Bennett J (1978) Calculation of the Avrami parameters for heterogeneous solid state reactions using a modification of the Kissinger method. Journal of Thermal Analysis 13: 283-292.
 12. ASTM (2013) G34: Standard test method for exfoliation corrosion susceptibility in 2xxx and 7xxx series aluminum alloys, ASTM.
 13. ASTM (1992) G110: Standard practice for evaluating intergranular corrosion resistance of heat treatable aluminum alloys by immersion in sodium chloride and hydrogen peroxide solutions, ASTM.
 14. Sheppard T (1999) Extrusion of Aluminum Alloys. Kluwer Academic Publications, Dordrecht, The Netherlands.
 15. Waterloo G, Hansen H, Gjønnnes J, Skjervold S (2001) Effect of predeformation and preaging at room temperature in Al-Zn-Mg-(Cu, Zr) alloys. Materials Science and Engineering 303: 226-233.